

A Multi-Kilowatt Immersion-Cooled Standard Electronic Clamshell Module for Future Aircraft Avionics

Peter E. Jimenez
Graduate Student

Issam Mudawar
Professor and Director.

Electronic Cooling Research Center,
Boiling and Two-Phase Flow Laboratory,
School of Mechanical Engineering,
Purdue University,
West Lafayette, IN 47907-1288

A new type of immersion cooled module, the BTPFL-C2, was developed for thermal management of future high flux avionics while conforming to the geometrical constraints of existing military modules and avionic enclosures. The BTPFL-C2 houses two circuit boards separated by a flow distribution plate and employs two sleeveless quick connection coolant couplers. The flow distribution plate supplies the coolant inside the module into parallel narrow channels formed between the distribution plate and the surfaces of the chips. Theoretical predictions of the thermal performance of the BTPFL-C2 were substantiated by experimental data using a test module populated with ten chips. Increasing the coolant subcooling at the module inlet was found to decrease pressure drop across the module, decrease the coolant flow rate requirements, and extend the upper cooling limit of the BTPFL-C2. These results reveal the BTPFL-C2 is capable of dissipating an order of magnitude more heat than today's most advanced avionic module. At an inlet subcooling of 40.3°C, the BTPFL-C2 could dissipate over 3000 W using only about 0.051 kg/s (0.50 gpm) of Fluorinert FC-72 and a pressure drop of only 2.8 kPa (0.41 psi).

Introduction

A combination of a large increase in the number of components integrated into today's high performance chips and a closer packaging of the chips in multi-chip boards has led to several order of magnitude increases in the rate of heat dissipation at the chip, board, and system levels in less than two decades. In the near future, present avionic cooling technology will be rendered obsolete by these compounding thermal problems.

Today, the majority of the SEM-E (Standard Electronic Module format-E) military avionic systems consist of an avionic enclosure packed with several modules. Each of these modules houses two circuit boards mounted back-to-back against a thermally conducting substrate which rejects the heat into the edges of the module. The heat is then rejected to air, which is bled directly from the compressor of the jet engine. These edge air cooled modules have an upper cooling limit of about 40 W. However, recent advances in avionic packaging have introduced modules which dissipate about 200 W (Barwick et al., 1991). This meant that the edge air cooling technologies have already fallen far behind even existing avionic needs. Since heat dissipation rates are expected to increase in the foreseeable future, the need already exists for more aggressive cooling schemes which are capable of keeping pace with the projected trends in device and board heat dissipation. Considering the

enormous development cost of military aircraft and the long time separating the commencement of aircraft design from actual deployment, it is imperative that any new cooling technology be capable of enduring at least two decades of the advances in device technology. Recognizing the complexity of this thermal management problem and its ramifications to the mission of future military aircraft, many U.S. defense agencies have set out in pursuit of innovative cooling schemes which could satisfy the stringent requirements of reduced system size and weight.

Edge air cooling modules conduct heat away from the device through a thermal bridge consisting of a solder layer, a thermal conducting substrate, and the two module guide rigs. The ribs are pressed against the walls of the avionic enclosure with the aid of special wedge screws. The heat is rejected to heat exchangers housed in the walls of the enclosure where it is convected by the air bled from the compressor. To reduce the thermal resistance inherent to edge air cooling, flow-through air cooling could be employed, where the air is routed through the module itself. However, flow-through air cooling would only produce a fractional increase in the module cooling rate over edge air cooling. Substantial increases in cooling rate can only be realized by substituting air with a liquid coolant. The liquid can be either circulated in the enclosure walls, edge liquid cooling, or pumped through the heat sink onto which the two circuit boards are mounted, flow-through liquid cooling. Both of these are classified as indirect liquid cooling techniques because the coolant does not come in direct contact with the

Contributed by the Electrical and Electronics Packaging Division for publication in the JOURNAL OF ELECTRONIC PACKAGING. Manuscript received by the EEPD August 1, 1993; revised manuscript received January 15, 1994. Associate Technical Editor: B. G. Sammakia.

device. Bowers and Mudawar (1993, 1994) utilized indirect cooling with phase change by soldering micro-channel and mini-channel heat sinks directly to the device. In their study, heat fluxes well above 150 W/cm^2 were recorded using R-113. Tuckerman and Pease (1981) also used micro-channel heat sinks but without phase change. The major drawback to their heat sink was the enormous pressure drop associated with the small diameter of the heat sink passages. Bowers and Mudawar demonstrated this problem can be alleviated, even with phase change, by employing mini-channels instead of micro-channels.

A more effective means of improving the thermal performance of avionic modules is to allow the coolant to assume intimate contact with the device and undergo phase change, thus eliminating the thermal resistance between the device and the coolant common to indirect liquid cooling schemes. Recently, Mudawar et al. (1994) developed a new type of SEM-E clamshell module, the BTPFL-C1 (named after Purdue's Boiling and Two-Phase Flow Laboratory), for the U.S. Navy using direct immersion cooling. The module consisted of an open cavity inside which two circuit boards were mounted to the module inner walls. Dielectric coolant FC-72 was supplied into the module and allowed to flow, undirected and at a very low speed, inside the module cavity before exiting the module to an external conditioning flow loop. The key design criteria for the module were to minimize coolant flow rate, minimize pressure drop, and ensure complete condensation of the vapor bubbles prior to exiting the module to the external loop. Mudawar et al. demonstrated the module could dissipate 820 W, four times the cooling rate of today's most powerful cooling module developed under the Air Force Pave program initiated in 1990 using indirect liquid cooling (see Mudawar et al., 1994).

To further enhance the thermal performance of the clamshell module developed earlier by Mudawar et al., designs other than an open cavity must be considered. Previous studies have revealed that, with phase change, the upper limit on device heat flux, critical heat flux (CHF), can be greatly ameliorated by (a) using enhanced surfaces which are formed directly in the device itself, or (b) by increasing the coolant velocity. The increase in coolant velocity can be easily attained by increasing the coolant flow rate. Nakayama et al. (1984) and Mudawar and Anderson (1993) used enhanced surfaces in saturated pool boiling and dissipated over 100 W/cm^2 , but due to size and weight constraints these enhanced surfaces cannot be used in an avionic module. Using jet impingement with a very high speed, Wadsworth and Mudawar (1992) dissipated more than 410 W/cm^2 . Alas, the stringent weight and size constraints of

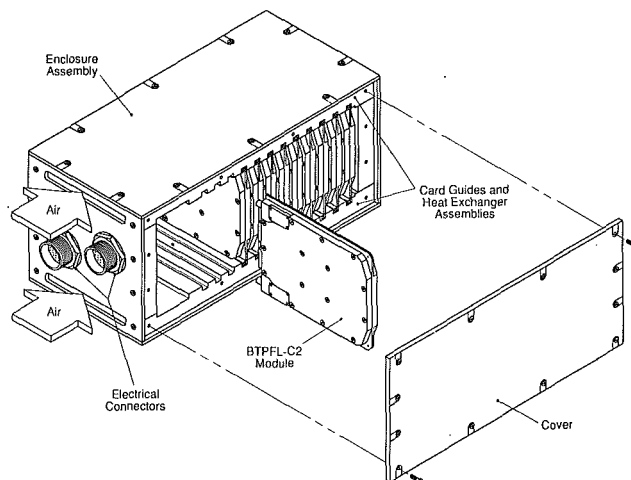


Fig. 1 Packing of BTPFL-C2 modules in a standard avionic enclosure

military aircraft preclude the use of a high capacity pump or a large coolant reservoir inside the avionic enclosure. However, increasing the coolant velocity can also be accomplished even with a small flow rate by reducing the flow area adjacent to the device surface. Notably, channeled flow with a moderate flow rate and high subcooling has been proven to dissipate over 100 W/cm^2 (Mudawar and Maddox, 1989).

The present study explores the effectiveness of direct immersion cooling and narrow channel flow at increasing the cooling rate of an SEM-E clamshell module for future avionic systems. Presented in this paper will be the design of this new module, the BTPFL-C2, and the thermal performance of the module populated with 32 of $1.27 \times 1.27 \text{ cm}^2$ chips. The analysis will include predictions of CHF limit and pressure drop across the module. The CHF predictions will be verified with experimental data obtained for a test module populated with a single chip and with a multitude of chips.

BTPFL-C2 Clamshell Module

Module Construction. Figure 1 illustrates how several BTPFL-C2 modules can be mounted side by side inside a standard avionic enclosure. Each module is held in place with wedge clamps attached to guide ribs protruding from the upper and lower edges of the module. The coolant enters the module through the back plate of the enclosure, and air, bled through

Nomenclature

A_{chip} = chip surface area ($1.27 \times 1.27 \text{ cm}^2$)		
A_F = channel cross-sectional area ($1.29 \text{ cm} \times 0.025 \text{ cm}$)	L_{SP} = difference between length of single-phase region and the entrance length for laminar boundary layer development	
c_p = specific heat at constant pressure	\dot{m}_{chip} = mass flow rate per chip	q'' = heat flux based on $1.27 \times 1.27 \text{ cm}^2$ chip surface area
D_F = hydraulic (friction) diameter (0.0498 cm)	\dot{m}_{mod} = mass flow rate of clamshell module	q_{mod} = heat dissipation rate of clamshell module
f_{fo} = single-phase friction factor	N = number of chips per module	q_m'' = critical heat flux based on $1.27 \times 1.27 \text{ cm}^2$ chip surface area
f_{TP} = two-phase friction factor	P = pressure	q_m^{**} = dimensionless critical heat flux defined in Eq. (6)
g = gravitational acceleration	P_h = heated perimeter (chip width, 1.27 cm)	Q_{chip} = volumetric flow rate per chip
G = mass velocity inside chip cooling channel, $\dot{m}_{\text{chip}}/A_F$	P_F = frictional perimeter (2.63 cm)	Q_{mod} = volumetric flow rate of clamshell module
h = enthalpy	ΔP = pressure drop across chip	Re_{D_F} = Reynolds number based
h_{fg} = latent heat of vaporization		
K_c = contraction loss coefficient		
K_e = expansion loss coefficient		
L = channel length (1.29 cm)		
L_{ent} = entrance length for lami-		

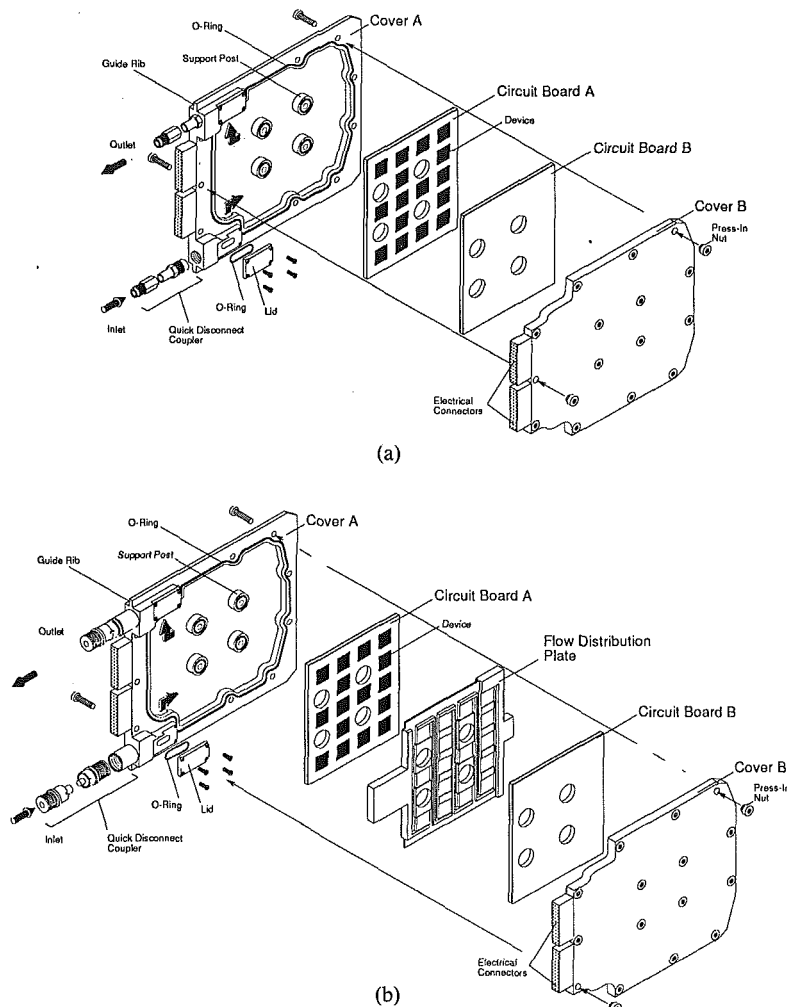


Fig. 2 Construction of (a) BTPFL-C1 and (b) BTPFL-C2

heat exchangers above and below the modules, extracts heat from the coolant and transports it out of the enclosure. A single enclosure may contain both low power conventional air cooled modules alongside a few BTPFL-C2 modules for the high-flux core processors, both types of modules have essentially the same outer geometrical envelope. A small cavity,

shown to the left of the enclosure, can be used to house the coolant pump and reservoir for the BTPFL-C2 modules. Alternatively, these coolant conditioning components could be located in a separate small enclosure.

Figures 2(a) and 2(b) show the BTPFL-C1, previously developed by the authors (Mudawar et al., 1994), and the BTPFL-

Nomenclature (cont.)

upon the channel hydraulic diameter, $G D_F / \mu_f$
 U = channel inlet velocity
 $U_{i,p}$ = inlet velocity of flow passage leading to chip cooling channel
 U_o = channel outlet velocity
 $U_{o,p}$ = outlet velocity of flow passage leaving the chip cooling channel
 T = temperature
 T_f = liquid temperature
 ΔT_{sat} = $T_w - T_{sat}$
 ΔT_{sub} = liquid subcooling, $T_{sat} - T_f$
 $\Delta T_{sub,i}$ = liquid subcooling at module inlet, $T_{sat} - T_i$
 $\Delta T_{sub,e}$ = liquid subcooling at module exit, $T_{sat} - T_e$
 ΔT_w = temperature difference be-

tween chip surface and liquid inlet, $T_w - T_i$
 U_m = mean velocity at a distance z from channel inlet
 v = specific volume
 v_{fg} = difference in specific volumes of saturated vapor and saturated liquid
 We = Weber number, $\rho_f U^2 L / \sigma$
 x_e = thermodynamic equilibrium quality
 z = coordinate in flow direction
 μ = dynamic viscosity
 ρ = density
 σ = surface tension

Subscripts

c = contraction

chip = chip
 D = fully developed single-phase boundary layer
 e = module exit; expansion
 f = liquid
 F = friction
 g = vapor
 h = heated
 i = module inlet
 m = mean
 mod = module
 o = channel outlet
 sat = saturation
 SP = single phase
 sub = subcooling
 U = developing single-phase boundary layer
 w = chip surface condition

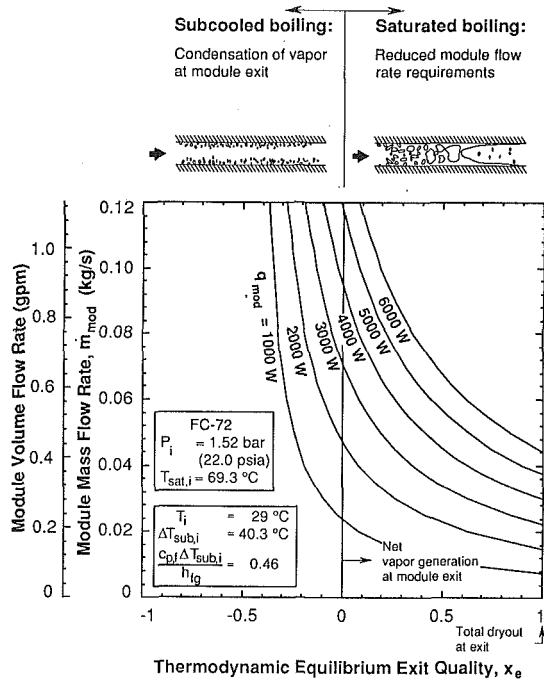


Fig. 3(a)

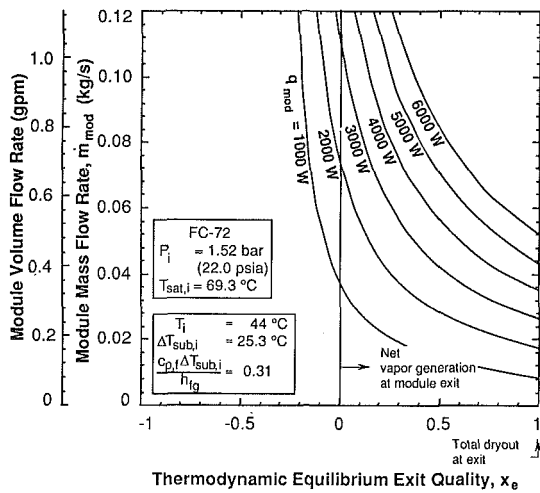


Fig. 3(b)

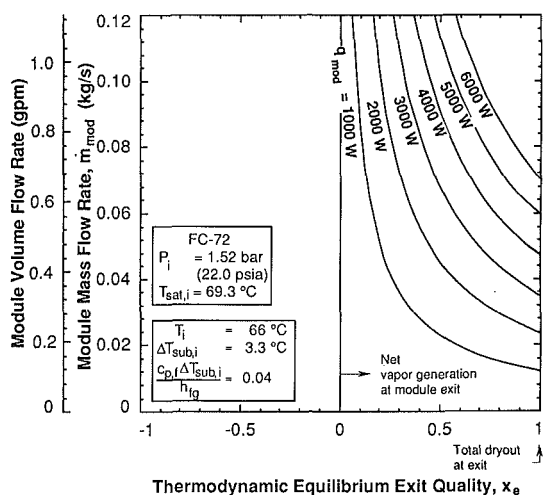


Fig. 3(c)

Fig. 3 Variation of module flow rate with thermodynamic equilibrium exit quality for different heat dissipation rates and inlet subcoolings of (a) 40.3°C, (b) 25.3°C, and (c) 3.3°C

C2, respectively. The outer clamshell of the BTPFL-C2 has an asymmetric design identical to that of the BTPFL-C1 and both are made of 7075-T6, an aluminum alloy with a high yield strength and good machinability. To correct its poor corrosion resistance, the module covers are treated with a chromate conversion finish. Each of the two modules houses two circuit boards which are mounted along the module inner walls. Two protrusions in cover A of each module allow the entire module thickness to be available for the coolant couplers. The coolant enters and exits the module cavity through two slots machined into the inlet and outlet protrusions, respectively. The primary difference between the two modules is the use of a flow distribution plate between the circuit boards of the BTPFL-C2 which creates a number of *parallel, narrow* channels formed between the flow distribution plate and the surfaces of the chips, coolant flows undirected inside the cavity of the BTPFL-C1. The flow distribution plate of the BTPFL-C2 can be easily fabricated by optically mapping the sizes and layout of the devices in the actual circuit board and reproducing the desired channel features with the aid of stereo-lithography. Another minor difference between the two modules is the type of sleeveless quick connection couplers used for the coolant. The Hydraflow DC2004 couplers used in the BTPFL-C1 are substituted with Aeroquip AE88720B couplers in the BTPFL-C2 due to the latter couplers' superior spillage and air inclusion characteristics. The relatively small outer envelope of the couplers used with either the BTPFL-C1 or the BTPFL-C2 place stringent constraints on the module's coolant flow rate. Pressure drop of both types of couplers increases appreciably above a flow rate of about 0.051 kg/s (0.50 gpm).

The size of the module cavity is maximized to provide adequate room for the circuit boards. Since the outer thickness has to conform to a military standard of 1.51 cm, the thickness of the module walls has to be greatly reduced which created structural problems. A stress analysis dictated that four support screws be used to prevent ballooning or catastrophic failure of the clamshell covers due to the internal pressure.

Thermal Design. While a primary objective of the BTPFL-C1 was the full condensation of vapor bubbles prior to exiting the module cavity, the objective of the BTPFL-C2 is to maximize the utilization of both the sensible and latent heat of the coolant by attempting to vaporize a large fraction of the flow rate. This objective was sought to facilitate a significant reduction in the flow rate requirements of the BTPFL-C2 for a given module heat dissipation rate or, alternatively, an increase in the rate of heat dissipation for a given flow rate when compared to the BTPFL-C1. Two important limits to the extent of coolant vaporization in the BTPFL-C1 are (i) catastrophic device failure due to CHF and (ii) excessive pressure buildup inside the module due to the two-phase friction and acceleration associated with the evaporating flow. These limits will be discussed in following sections.

The most common measure of the extent of fluid vaporization in a channel is thermodynamic equilibrium quality. At the module exit, the thermodynamic equilibrium quality, x_e , can be calculated using the following equation

$$x_e = \frac{q_{mod}}{\dot{m}_{mod} h_{fg}} - \frac{c_p \Delta T_{sub,i}}{h_{fg}} \quad (1)$$

Figures 3(a)–3(c) show the variation of x_e with module flow rate for module heat dissipation rates between 1000 and 6000 W using Fluorinert FC-72. The three figures depict a sharp reduction in coolant flow rate is possible if larger values of x_e can be tolerated. The schematics in Fig. 3(a) summarize the fundamental difference between the BTPFL-C1 and the BTPFL-C2 modules, the first is designed to operate with negative x_e values (i.e., condensed exit flow) and the second positive x_e values (i.e., saturated exit flow with a large vapor production). Figure 3(a) shows allowing total dryout at the

module exit ($x_e = 1$) would enable the BTPFL-C2 to dissipate 1000 W using one third the flow rate of the BTPFL-C1. Comparing Figs. 3(a) through 3(b) reveals decreasing coolant subcooling at the module inlet increases the flow rate required to attain a given value of x_e . Figure 3(c) shows a near-saturated inlet flow demands the largest flow rates and creates operating conditions the BTPFL-C1 cannot tolerate.

CHF Limit. The performance envelope for the BTPFL-C1 was developed using the criteria for zero net vapor generation at the module exit, $x_e \leq 0$, and CHF, as predicted, due to the low coolant velocities inside the cavity of the BTPFL-C1, by the Mudawar and Anderson correlation (1990) for stagnant (i.e., pool boiling) conditions.

$$\frac{q_m''}{q_{m, \text{sat}}''} = 1 + 0.0643 \left(\frac{\rho_g}{\rho_f} \right)^{0.25} \frac{\rho_f c_{p, f} \Delta T_{\text{sub}, e}}{\rho_g h_{fg}} \quad (2)$$

where $\Delta T_{\text{sub}, e}$ is the difference between the saturation temperature and module exit temperature, which was calculated by performing a sensible heat balance on the entire module.

$$T_e - T_i = \frac{q_{\text{mod}}}{\dot{m}_{\text{mod}} c_{p, f}} \quad (3)$$

The CHF values for saturated pool boiling, $q_{m, \text{sat}}''$, were obtained using the equation developed by Zuber et al. (1961),

$$q_{m, \text{sat}}'' = 0.131 \rho_g h_{fg} \left(\frac{\sigma g (\rho_f - \rho_g)}{\rho_g^2} \right)^{0.25} \quad (4)$$

Combining Eqs. (2) and (3) gives

$$q_m'' = \frac{q_{m, \text{sat}}'' \left[1 + 0.0643 \left(\frac{\rho_g}{\rho_f} \right)^{0.25} \frac{\rho_f c_{p, f} \Delta T_{\text{sub}, i}}{\rho_g h_{fg}} \right]}{1 + 0.0643 q_{m, \text{sat}}'' \left(\frac{\rho_g}{\rho_f} \right)^{0.25} \frac{\rho_f N A_{\text{chip}}}{\rho_g h_{fg} \dot{m}_{\text{mod}}}} \quad (5)$$

where N and A_{chip} are the total number of chips inside the module and the chip surface area, respectively.

CHF values for the BTPFL-C2 module were based on the Mudawar and Maddox (1989) correlation for channel flow boiling.

$$q_m^{**} = \frac{q_m'' / (\rho_g U h_{fg})}{\left(\frac{\rho_f}{\rho_g} \right)^{15/23} \left(\frac{L}{D_F} \right)^{1/23} \left(1 + \frac{c_{p, f} \Delta T_{\text{sub}, i}}{h_{fg}} \right)^{1/23} \left(1 + 0.021 \frac{\rho_f c_{p, f} \Delta T_{\text{sub}, i}}{\rho_g h_{fg}} \right)^{16/23}} = 0.161 \left(\frac{\sigma}{\rho_f U^2 L} \right)^{8/23} \quad (6)$$

Since net vapor generation at the module exit is not a concern for the BTPFL-C2, the entire performance envelope for this module is determined solely by the CHF limit.

Figure 4(a)–(4c) show numerical results based on the net vapor generation limit and the two CHF limits for a module fully populated with 32 of $1.27 \times 1.27 \text{ cm}^2$ chips and having chip cooling channels with a 0.025 cm gap thickness. Shown shaded in each figure is the performance envelope for the BTPFL-C1 prescribed at low flow rates by the net vapor generation limit and at high flow rates by the CHF limit based on the Mudawar and Anderson correlation. A significant widening of the envelope in the direction of higher module heat dissipation rates is attainable with the BTPFL-C2 due to the higher CHF values possible with increased coolant velocity. For example, the flow rate of 0.051 kg/s (0.50 gpm) (upper recommended limit for fluid couplers) and 40.3 °C inlet subcooling enable the BTPFL-C2 to dissipate over 300 W, about three times that of the BTPFL-C1 and 15 times that of the Air Force Pave module. Comparing Figs. 4(a) through 4(c) reveals decreasing the inlet subcooling decreases the cooling capability of both modules, the effect being more drastic for the BTPFL-C1, especially for the near saturated case, Fig. 4(c).

Pressure Drop. A large pressure drop across the module greatly increases the operating pressure inside the module cavity which can lead to catastrophic failure of the module walls if the yield strength is exceeded. Increasing pressure drop would also adversely affect the weight of the coolant reservoir and the weight and power consumption of the pump. Since the BTPFL-C2 is designed to evaporate much of the flow, concern over such effects as excessive flashing and compressibility (and even choking) of the two-phase flow demanded accurate modeling of the pressure drop characteristics of the module.

A mathematical model is presented which predicts the pressure drop across a single chip cooling channel for varying flow rates and chip heat fluxes. Since the channels are machined in a parallel cooling configuration and the flow resistances in the module inlet and outlet couplers and the relatively large passages leading to and from the chip channels are negligible, the channel pressure drop is essentially equal to the entire module pressure drop.

The model was developed for a channel which is uniformly heated on one side (along the chip surface). The channel length consists of three regions: (i) an upstream developing single-phase region where $x_e \leq 0$, (ii) a fully developed single-phase region extending from the end of the upstream developing region to the location corresponding to the saturated state, $x_e = 0$, and (iii) a two-phase region from the $x_e = 0$ location to the channel outlet. This model calculates pressure drop for the single-phase and two-phase regions separately and accounts for both flashing and compressibility in the two-phase region.

Two-Phase Pressure Drop. Vaporization in the two-phase region greatly accelerates the flow causing an increase in the pressure gradient as compared to the single-phase region. The homogeneous equilibrium model was used to predict the pressure drop in the two-phase region. This model assumes uniform and equal velocities of the liquid and vapor, a uniform pressure across the flow area, and uniform properties for each phase across the flow area. In addition, the temperature of the two-phase mixture is assumed uniform and equal to the saturation temperature corresponding to the local pressure.

At any distance z from the channel inlet, mass conservation yields

$$\frac{d}{dz} (A_F G) = 0, \quad (7)$$

Thus, mass velocity, G , is constant in the direction of fluid flow since A_F is constant. Since the mixture density greatly decreases due to axial vaporization along the channel, the mixture velocity, U_m , should increase.

Conservation of momentum for a channel differential control volume of length dz gives

$$-\left(\frac{dP}{dz} \right) = \frac{1}{2} \frac{P_F}{A_F} f_{TP} G^2 (v_f + x_e v_{fg}) + G \frac{dU_m}{dz}, \quad (8)$$

where f_{TP} , which was set equal to 0.005, is the two-phase friction factor and P_F is the frictional perimeter. Equation (8) shows the pressure gradient as a sum of a frictional term and an accelerational term, respectively.

Energy conservation for the same control volume yields

$$G A_F \frac{d}{dz} \left(h + \frac{U_m^2}{2} \right) = q'' P_h, \quad (9)$$

where P_h is the heated perimeter of the channel (i.e., chip width) and the enthalpy, h , is given by

$$h = h_f + x_e h_{fg}. \quad (10)$$

Since $U_m = G(v_f + x_e v_{fg})$, and assuming that the properties are uniquely determined by the local pressure, P , Eqs. (8) and (9) can be rewritten, respectively, as

$$-\left(\frac{dP}{dz}\right) = \frac{1}{2} \frac{P_F}{A_F} f_{TP} G^2 (v_f + x_e v_{fg}) + G^2 \left[v_{fg} \frac{dx_e}{dz} + \frac{dP}{dz} \left(\frac{dv_f}{dP} + x_e \frac{dv_{fg}}{dP} \right) \right] \quad (11)$$

$$\frac{dx_e}{dz} = \frac{\frac{q'' P_h}{GA_F} + \left[G^2 (v_f + x_e v_{fg}) \left(\frac{dv_f}{dP} + x_e \frac{dv_{fg}}{dP} \right) + \left(\frac{dh_f}{dP} + x_e \frac{dh_{fg}}{dP} \right) \right] \left(-\frac{dP}{dz} \right)}{h_{fg} + G^2 v_{fg} (v_f + x_e v_{fg})}. \quad (12)$$

Equation (12) determines the change in quality in the axial direction, accounting for flashing, due to variations in vapor and liquid enthalpies with pressure, and compressibility, due to variations in vapor and liquid specific volumes with pressure.

Solving Eq. (11) for $-dP/dz$ gives

$$-\frac{dP}{dz} = \frac{\frac{1}{2} \frac{P_F}{A_F} f_{TP} G^2 (v_f + x_e v_{fg}) + G^2 v_{fg} \frac{dx_e}{dz}}{1 + G^2 \left(\frac{dv_f}{dP} + x_e \frac{dv_{fg}}{dP} \right)}. \quad (13)$$

Equation (13) predicts the pressure gradient in the axial direction resulting from friction along the channel walls, acceleration of the fluid due to phase change, and compressibility.

Equations (12) and (13) were solved simultaneously using the fourth-order Runge-Kutta technique to determine local values of equilibrium quality and pressure in the two-phase region.

Single-Phase Pressure Drop. The pressure drop in the single-phase regions is the sum of pressure drop in the upstream developing flow region, where the velocity profile is changing, and pressure drop in the fully-developed region, where the velocity profile is constant. The entrance length for the laminar developing region is given by (see Bowers and Mudawar, 1993)

$$L_{ent} = 0.05 \text{ Re}_{D_F} D_F. \quad (14)$$

Using L_{ent} from Eq. (14), the pressure drop for the developing region was calculated by using the Blasius equation (Schlichting, 1955) which yields

$$\Delta P_U = \frac{2.66 G^{1.5}}{\rho_f D_F} \sqrt{L_{ent} \mu_f}. \quad (15)$$

From $z = L_{ent}$ to the location where $x_e = 0$, the pressure drop was determined using the equation for pipe friction in fully-developed flow.

$$\Delta P_D = \frac{2 f_{f_0} G^2 L_{SP}}{D_F \rho_f}, \quad (16)$$

where $f_{f_0} = 16/\text{Re}_{D_F}$. The total pressure drop in the single-phase regions is the sum of the pressure drop in the developing and fully developed regions,

$$\Delta P_{SP} = \Delta P_U + \Delta P_D. \quad (17)$$

Expansion and Contraction Pressure Drops. At the inlet and outlet of the channel, pressure drops associated with the sudden change in flow area were calculated using the following relations (Todreas and Kazimi, 1990):

$$\Delta P_c = \frac{(U^2 - U_{i,p}^2)}{2v_f} + \frac{K_c U^2}{2v_f}, \quad (18)$$

$$\Delta P_e = \frac{(U_{o,p}^2 - U_o^2)}{2(v_f + x_e v_{fg})} + \frac{K_e U_o^2}{2(v_f + x_e v_{fg})}. \quad (19)$$

where K_e and K_c are, respectively, the expansion and contraction coefficients based on the channel geometry and the area ratio at the channel inlet and outlet, U and U_o are the channel inlet and outlet velocities, respectively, and $U_{i,p}$ and $U_{o,p}$ are, respectively, the velocities in the flow passages leading to and from the channel inlet and outlet.

Figures 5(a)–5(c) display pressure drop predictions for different chip heat fluxes and the CHF values calculated using the Mudawar and Maddox correlation (1989) for inlet subcoolings of 40.3, 25.3, and 3.3°C. At low flow rates, the two-phase region occupies most of the channel length and, for each heat flux value, the pressure drop increases with increasing flow rate due to increases in both the frictional and accelerational components of the two-phase pressure gradient. As the flow rate is increased further, ΔP attains a maximum before starting to decrease due to a larger fraction of the channel length remaining in the single-phase region. ΔP then reaches a minimum where the entire channel is in the single-phase regime. Additional increases in flow rate beyond the minimum point increase friction in essentially a single-phase liquid flow, resulting in a corresponding increase in ΔP . Figures 5(a)–5(c) show increasing chip heat flux and/or decreasing the inlet subcooling increase the channel pressure drop. Each of the three figures also includes pressure drop predictions corresponding to CHF. The CHF pressure drop is the upper limit for pressure drop which can be attained safely without the risk of chip burnout. Note that for single-phase liquid flow (high flow rates), CHF occurs due to the formation of a very thin vapor layer at the chip surface while the bulk flow is essentially subcooled liquid.

Experimental Methods

To validate the predicted thermal performance of the BTPFL-C2 module, boiling curves and CHF data were obtained for a single chip inside a *test module* using Fluorinert FC-72. Additional data were then obtained with the same test module populated with ten chips to determine if the performance of a single chip is representative of a fully populated module.

Construction and Instrumentation of Test Module. The test module was an all aluminum module consisting of cover A and cover B similar to those shown in Fig. 2(b), but with a single circuit board. The circuit board carried ten individually powered simulated chips as shown in Figs. 6(a) and 6(b).

The coolant was guided to the simulated chips by an aluminum flow distribution plate shown in Fig. 7(a). The coolant passed through a 0.500 cm × 0.787 cm channel which branched into two smaller 0.500 cm × 0.508 cm passages. Each of the two smaller passages directed the coolant to five of 1.29 cm × 0.025 cm parallel narrow channels formed between the distribution plate itself and the chip surfaces. The fluid then departed the narrow channels and exited the flow distribution plate through passages identical to those leading to the ten channels.

Each of the simulated chips consisted of a 1.27 × 1.27 cm² oxygen-free copper slab protruding 0.0254 cm from the carrier

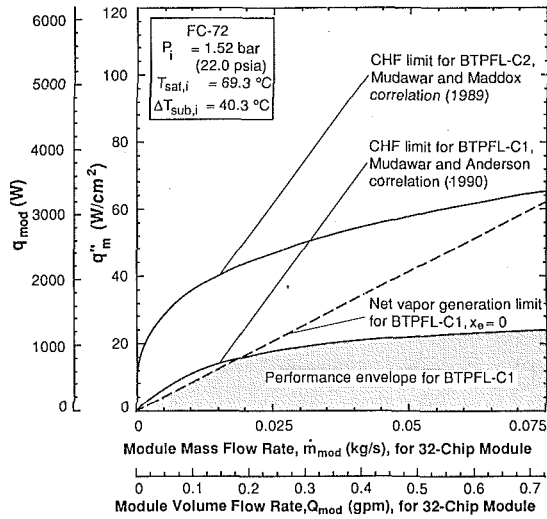


Fig. 4(a)

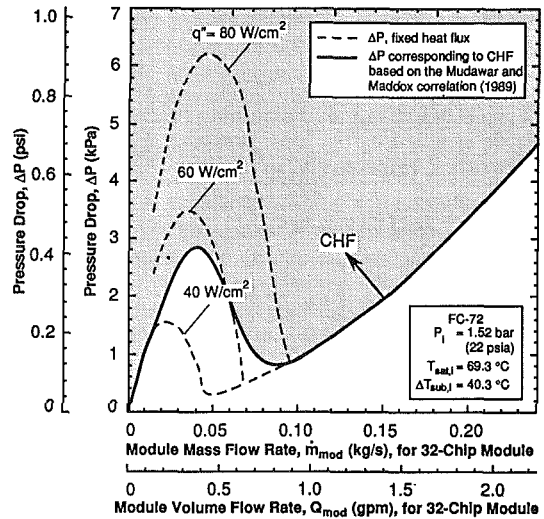


Fig. 5(a)

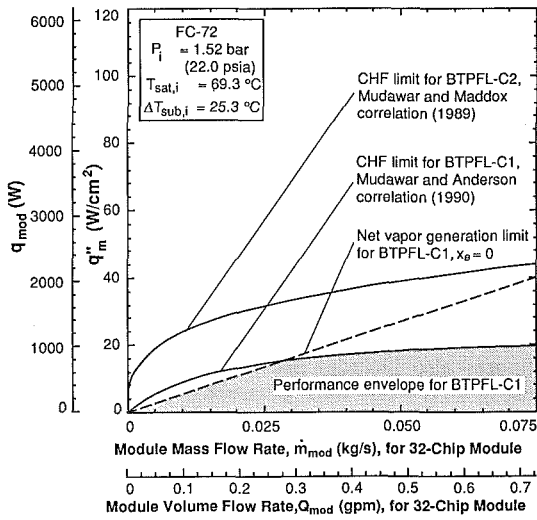


Fig. 4(b)

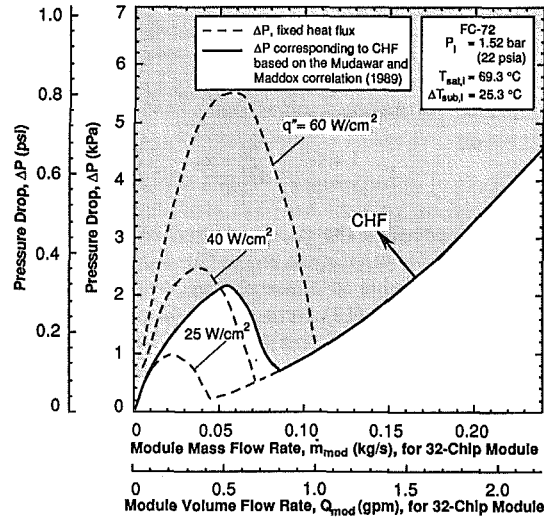


Fig. 5(b)

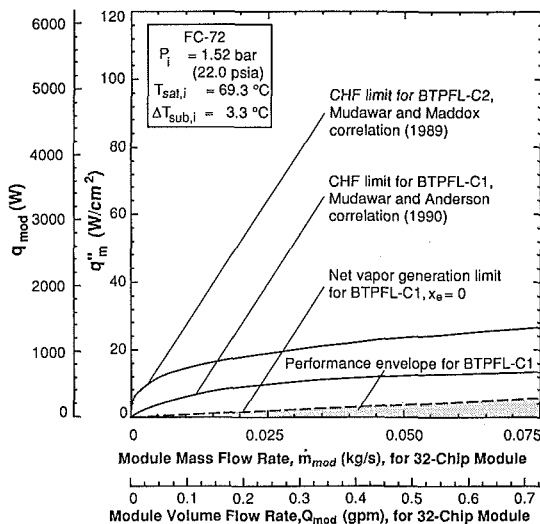


Fig. 4(c)

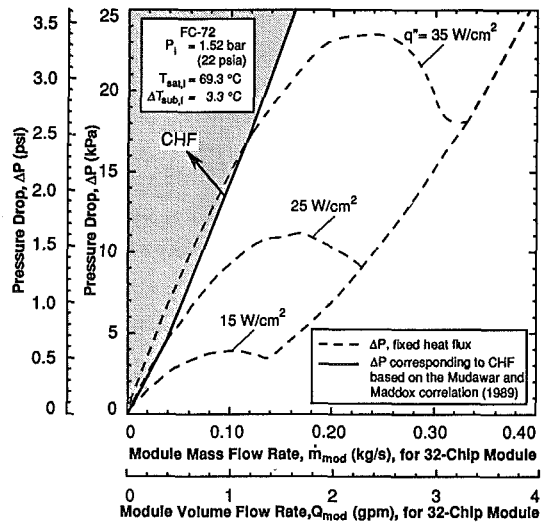


Fig. 5(c)

Fig. 4 Variation of chip CHF and BTPFL-C2 heat dissipation rate with flow rate for a module housing two circuit boards, each carrying 16 of 1.27×1.27 cm² chips for inlet subcoolings of (a) 40.3°C, (b) 25.3°C, and (c) 3.3°C

Fig. 5 Variation of pressure drop across the BTPFL-C2 module with flow rate for different chip heat fluxes and for CHF values based upon the Mudawar and Maddox correlation (1989) for inlet subcoolings of (a) 40.3°C, (b) 25.3°C, and (c) 3.3°C

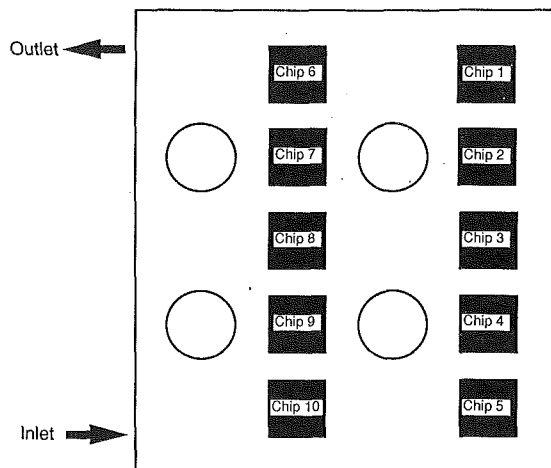


Fig. 6 (a)

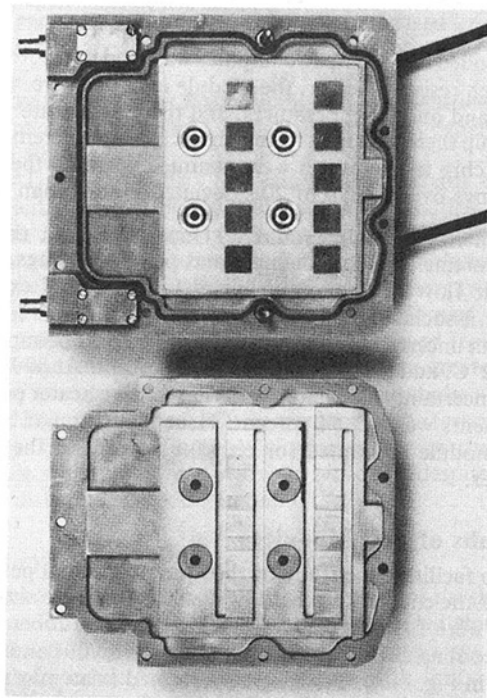


Fig. 6 (b)

Fig. 6 (a) Layout of simulated chips in test module and (b) photographs of BTPFL-C2 cover A (above) including the simulated chips and cover B (below) containing the flow distribution plate

plate. Heat was provided to the chip by a $90\ \Omega$ thick film resistive heater which was silver soldered to the underside of the copper slab as shown in Fig. 7(b). The temperature of each chip was measured by a Chromel-Alumel thermocouple embedded 0.145 cm below the chip surface. One-dimensional heat conduction was assumed in extrapolating the chip surface temperature. As shown in Fig. 7(b), the resistive heaters and copper slabs were mounted onto a G-7 fiberglass support platform which rested upon a back plate also made of G-7. An aluminum rim enclosed the entire circuit board and a G-7 cover plate was used to hold the chips in place and conceal the chip power leads and thermocouple wires.

The instrumentation wires were routed through two openings in cover A and through an aluminum connector block attached to the back of cover A. The connector block was fitted with two Pave stainless steel pass thru electrical connectors which had wires extending on both sides of a hermetic seal. The wires external to the module were connected to the data acquisition system and a 240-Vac auto-transformer.

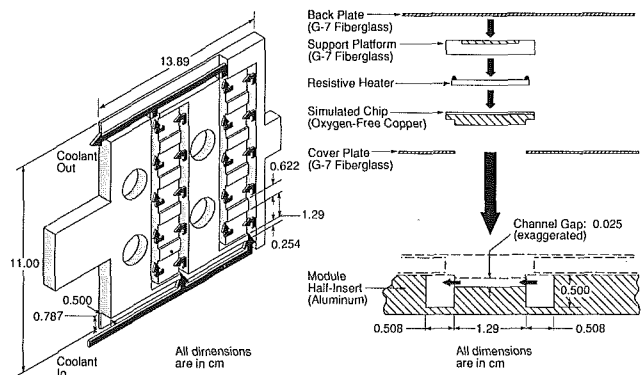


Fig. 7 Schematic of coolant flow (a) through half insert of test module and (b) over a single chip

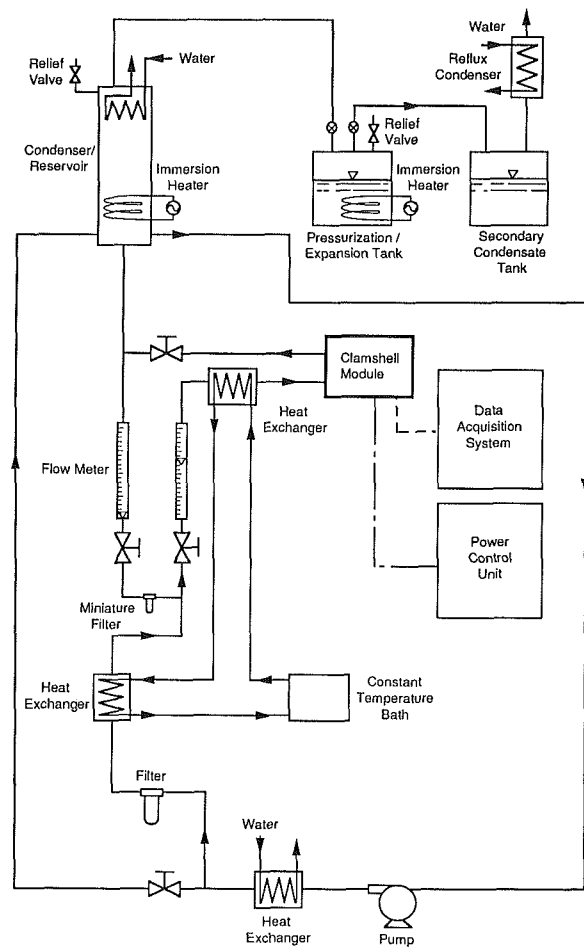


Fig. 8 Two-phase flow loop

The test module was contained in a cardguide which simulated the enclosure in which an actual BTPFL-C2 module would be inserted, Fig. 1. The module was secured in the cardguide with wedge clamps and the back plate of the cardguide contained fluid coupler parts which mated with those in the module.

Flow Loop. Figure 8 shows a diagram of the two-phase flow loop which was used to measure the performance of the test module. The coolant was circulated through the loop by a magnetically coupled centrifugal pump. After exiting the pump a small portion of the flow was bypassed and entered one of two flowmeters located upstream of the test module. The coolant then passed through the module, remixed with

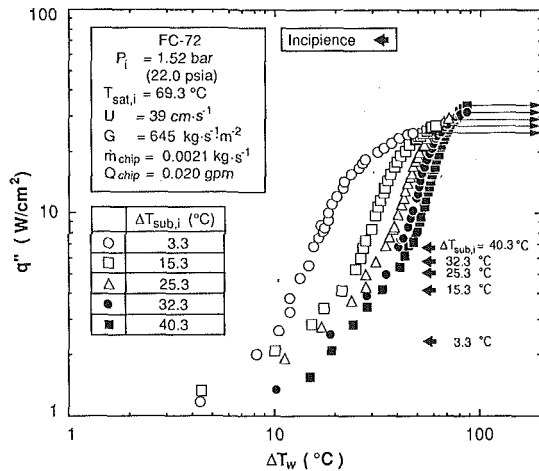


Fig. 9 Boiling curves for Chip 8 for a chip flow rate of 0.0021 kg/s and different inlet subcoolings

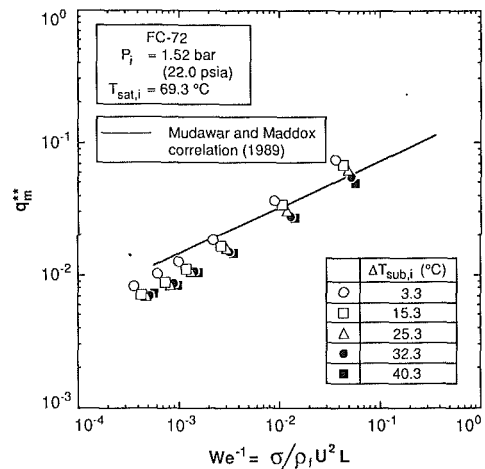


Fig. 11 Comparison of CHF data with predictions based on the Mudawar and Maddox correlation (1989)

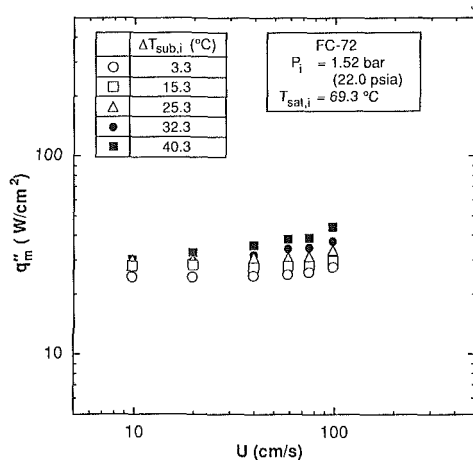


Fig. 10 Critical heat flux versus channel velocity for different subcoolings

the previously bypassed fluid, and emptied into the loop condenser/reservoir.

The fluid temperature was regulated by a cold water heat exchanger located immediately downstream of the pump and two constant-temperature baths, one located before the module inlet and another preceding the flowmeters. Coarse adjustment of the system pressure was accomplished by a water-cooled condenser coil submerged in the condenser/reservoir and by immersion heaters located in the pressurization/expansion tank. Fine tuning of the pressure was achieved with the aid of two regulating valves, one located downstream of the module outlet and the other just upstream of the flowmeters.

The module inlet and outlet temperatures were monitored by thermocouples placed just upstream and downstream of the module inlet and outlet ports. The module inlet pressure was measured by a Sensotec absolute pressure transducer.

Operating Procedure. The coolant was deaerated in the flow loop for 20 minutes prior to data taking by boiling the coolant using the immersion heaters situated inside the loop condenser/reservoir. Pressure buildup in the condenser/reservoir forced the FC-72 vapor and noncondensable gases through the pressurization/expansion tank and into the secondary condensate tank where the noncondensable gases were expelled from the system as the FC-72 vapor was recovered by a water-cooled reflux condenser.

While maintaining the desired module inlet pressure and temperature, the power to each resistive heater was increased in very slow increments. A Keithley 500 data acquisition system

controlled by a Compaq computer was used to record the power of each resistive heater, the module inlet pressure, the module inlet and outlet temperatures, and the steady-state voltages of the chip thermocouples following each power increment. Steady state chip temperatures were assumed when 20 thermocouple readings over a span of 20 s deviated by less than 0.1°C.

Experimental Uncertainty. Uncertainties in the pressure measurements, thermocouple and power readings, and volumetric flow rates all contributed to the global experimental error associated with each reading. The pressure transducer had an uncertainty of ± 0.0103 bar, the thermocouple readings $\pm 0.2^\circ\text{C}$, and the flowmeters ± 1.6 percent. At 80 W per chip, the uncertainty associated with the resistive heater power measurements was ± 2.54 percent. Heat loss through the back of the module accounted for only 0.8 percent of the chip input power.

Results of Test Module

To facilitate the study of the module thermal performance, all of the channels in the flow distribution plate shown in Fig. 7(a) were first blocked with RTV silicone rubber except for the cooling channel of Chip 8 (see chip layout and nomenclature in Fig. 6(a)). Tests were performed at an inlet pressure of 1.52 bar, corresponding to a saturation temperature of 69.3°C, and chip flow rate and subcooling ranges of 0.0005–0.0053 kg/s and 3.3–40.3°C, respectively. Once the thermal characterization of a single chip was completed, all of the channels were cleared from the RTV and experiments were performed on the test module populated with the ten chips to verify the results of a single chip were representative of those in a fully populated module.

Boiling Curves. Figure 9 shows boiling curves for Chip 8 at a chip flow rate of 0.0021 kg/s (0.0020 gpm) and inlet subcoolings between 3.3 and 40.3°C. For all of the flow rates tested, increased subcooling delayed incipience to higher heat fluxes, increased critical heat flux, and slightly decreased the chip surface temperature; however, since the heat flux is plotted versus ΔT_w rather than ΔT_{sat} , the increase in subcooling causes the boiling curves to shift to the right.

Critical Heat Flux. A plot of critical heat flux versus channel velocity for subcoolings between 3.3 and 40.3°C is shown in Fig. 10. Increasing velocity and/or subcooling yielded an increase in CHF due to a reduction in bubble size and an increased access of bulk liquid to the chip surface. The effect of increasing subcooling on CHF was less pronounced at smaller velocities where the coolant reached its saturation temperature

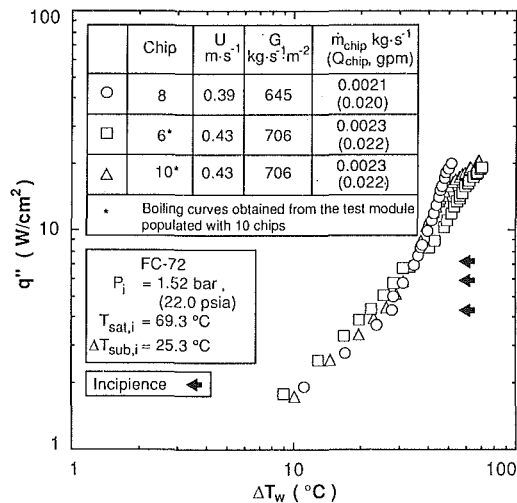


Fig. 12 Comparison of boiling performance of Chip 8 from single chip test and of Chips 6 and 10 from ten chip test at 25.3°C inlet subcooling

closer to the channel inlet, thus eliminating the significance of the coolant sensible energy and the advantages inherent to subcooled flow.

Figure 11 compares the CHF values measured for Chip 8 with predictions based on the Mudawar and Maddox (1989) correlation. At low velocities (greater values along the x -axis), the data are in reasonable agreement with the correlation, but at higher velocities the data show some deviation from the correlation. This deviation could be attributed, in part, to the Mudawar and Maddox correlation being developed from chip data inside a channel having a hydraulic diameter greater than that of the narrow channel used in the present study.

Figure 12 shows the thermal performance of the test module containing Chip 8 alone is fairly similar to that of the same test module when populated with the ten chips despite some deviation at fluxes exceeding about 15 W/cm².

Conclusions

Experimental data and theoretical predictions of the thermal performance of a new two-phase immersion cooled clamshell module, the BTPFL-C2, were obtained to explore the suitability of this module for cooling of future high flux aircraft avionics. Key conclusions from this study are as follows:

(1) Allowing net vapor generation at the module outlet greatly decreases the coolant flow rate requirements for a given module heat dissipation rate compared to a module with a condensed outlet flow.

(2) The module pressure drop and flow rate requirements

can be greatly reduced by increasing the coolant subcooling at the module inlet.

(3) The upper cooling limit of the BTPFL-C2 due to CHF can be extended by increasing the inlet subcooling.

(4) The module CHF data showed a fair agreement with the predictions of the Mudawar and Maddox correlation (1989). Thus, this correlation is recommended for setting upper limits for cooling with the BTPFL-C2.

(5) Perhaps the most important conclusion from this study is the ability of the BTPFL-C2 to dissipate more than an order of magnitude more heat than today's most advanced indirect liquid cooled Air Force Pave module (which is rated at about 200 W). For example, at an inlet subcooling of 40.3°C, the BTPFL-C2 can dissipate over 3000 W using only about 0.051 kg/s (0.50 gpm) of Fluorinert FC-72 and a corresponding pressure drop of only 2.8 kPa (0.41 psi).

References

- Barwick, M., Midkoff, M., and Seals, D. 1991, "Liquid Flow-Through Cooling for Avionics Applications," *Proc. IEEE 1991 National Aerospace and Electronics Conf.*, (NAECON), Vol. 1, Dayton, Ohio, pp. 227-230.
- Bowers, M. B., and Mudawar, I., 1993, "Two-Phase Electronic Cooling Using Mini-Channel and Micro-Channel Heat Sinks-Part 2. Flow Rate and Pressure Drop Constraints," *Proc. ASME Int. Electronics Packaging Conference*, Vol. 2, pp. 703-712.
- Bowers, M. B., and Mudawar, I., 1994, "High Flux Boiling in Low Flow Rate, Low Pressure Drop Mini-Channel and Micro-Channel Heat Sinks," *Int. J. Heat Mass Transfer*, Vol. 37, pp. 321-332.
- Mudawar, I., and Anderson, T. M., 1990, "Parametric Investigation into the Effects of Pressure, Subcooling, Surface Augmentation and Choice of Coolant on Pool Boiling in the Design of Cooling Systems for High-Power Density Chips," *ASME JOURNAL OF ELECTRONIC PACKAGING*, Vol. 112, pp. 375-382.
- Mudawar, I., and Anderson, T. M., 1993, "Optimization of Enhanced Surfaces for High Flux Chip Cooling by Pool Boiling," *ASME JOURNAL OF ELECTRONIC PACKAGING*, Vol. 115, pp. 89-100.
- Mudawar, I., and Jimenez, P. E., and Morgan, R. E., 1994, "Immersion-Cooled Standard Electronic Clamshell Module: A Building Block for Future High-Flux Avionic Systems," *ASME JOURNAL OF ELECTRONIC PACKAGING*, Vol. 116, pp. 116-125.
- Mudawar, I., and Maddox, D. E., 1989, "Critical Heat Flux in Subcooled Flow Boiling of Fluorocarbon Liquid on a Simulated Electronic Chip in a Vertical Rectangular Channel," *Int. Journal of Heat Mass Transfer*, Vol. 32, pp. 379-394.
- Nakayama, W., Nakajimi, T., and Hirasawa, S., 1984, "Heat Sink Studs Having Enhanced Boiling Surfaces for Cooling of Microelectronic Components," *ASME Paper 84-WA/HT-89*.
- Schlichting, H., 1955, *Boundary Layer Theory*, McGraw-Hill, New York, pp. 22-25.
- Todreas, N. E., and Kazimi, M. S., 1990, *Nuclear Systems I*, Hemisphere Publishing, New York, pp. 398-403.
- Tuckerman, D. B., and Pease, R. F. W., 1981, "High-Performance Heat Sinking for VLSI," *IEEE Electron Device Letters*, Vol. EDL-2, pp. 126-129.
- Wadsworth, D. C., and Mudawar, I., 1992, "Enhancement of Single-Phase Heat Transfer and Critical Heat Flux from an Ultra-High-Flux Simulated Microelectronic Heat Source to a Rectangular Impinging Jet of Dielectric Liquid," *ASME Journal of Heat Transfer*, Vol. 114, pp. 764-768.
- Zuber, N., Tribus, M., and Westwater, J. W., 1961, "The Hydrodynamic Crisis in Pool Boiling of Saturated and Subcooled Liquids," *Int. Developments in Heat Transfer*, Part 2, ASME, pp. 230-236.